ELECTRONIC SUPPLEMENTARY INFORMATION

for

Hydrogermylation initiated by trialkylborohydrides: a living anionic mechanism

Maciej Zaranek
Centre for Advanced Technologies
Adam Mickiewicz University
Uniwersytetu Poznanskiego St. 10
61-614 Poznan, Poland
m.zaranek@amu.edu.pl

Mateusz Nowicki
Faculty of Chemistry
Adam Mickiewicz University
Uniwersytetu Poznanskiego St. 8
61-614 Poznan, Poland

Piotr Andruszak
Faculty of Chemistry
Adam Mickiewicz University

Marcin Hoffmann
Faculty of Chemistry
Adam Mickiewicz University

Piotr Pawluć
Centre for Advanced Technologies
& Faculty of Chemistry
Adam Mickiewicz University

Contents

1. Methods

1.1. DFT calculations

Initial structures of phenylsilane, phenylgermane, diphenylgermane, triethylgermane, styrene, sodium trimethylborohydride and sodium borohydride were generated with usual values of bond lengths and valence angles[1] and were followed by full geometry optimization toward potential energy minima. In these and subsequent computations, M06-2X/6-31++G(d,p)/LANL2DZdp level of theory[2,3,12,4–11] was employed (LANL2DZdp basis set for Si and Ge atoms and 6-31++G(d,p) for other atoms); this selection was dictated by our previous research on similar reactions[13] on the one hand, and by an attempt to accurately describe the behaviour of outer shell electrons in Si and Ge atoms while maintaining a similar structure of basis set (both are valence double-zeta basis sets with additional polarization and diffuse functions) and an acceptable level of computing power and disk space consumption. Based on our previous research, triethylborane was substituted with trimethylborane in order to reduce computational complexity at a negligible change in relative energies of respective structures. In order to identify possible reaction pathways, we conducted relaxed potential energy scans while controlling 1 or 2 interatomic distances. Whenever a scan did not result in a new stationary point, the path was discarded; otherwise, synchronous transit-guided quasi-Newton approach (**QST3**)[14] was used to determine the geometry of the respective transition state (TS), followed by a pseudo **IRC**[15] calculation to confirm or generate potential energy minima that are connected by a given TS. For all stationary points identified throughout the research, force constants and the resulting vibrational modes (**freq** calculations) were computed; these comprised either zero or one imaginary frequency, the former corresponding to potential energy minima and the latter corresponding to first-order saddle points (transition states). Each of those calculations was carried out for molecules dissolved in toluene (as was the case in the experimental part) within the polarizable continuum model (PCM).[16,17,26–34,18–25] For thermochemical calculations, standard pressure p=1.00000 atm and temperature T=373.150 K were applied. These conditions were used in order to genuinely reproduce the experimental environment. Finally, to account for the large differences in the number of atoms between individual systems, Boys-Bernardi counterpoise method[35,36] was used for minimizing basis set superposition error. Up to four fragments were specified, depending on system size, out of the following blocks: sodium hydride, trimethylborane, styrene, phenylsilane/phenylgermane/diphenylgermane/triethylgermane. Gaussian 16 program package was used for all quantum-chemical computations throughout our research.[37] Basis Set Exchange resource was used to optimize the level of theory employed.[38]

1.2. General remarks for experimental procedures

All reactions were performed in an oven-dried glassware under the argon atmosphere. Solvents were dried by distillation over sodium/benzophenone. Styrenes (Merck / Sigma-Aldrich) and germananes (GelEst Inc.) were used as supplied and degassed prior to use. Alkali metal trialkylborohydrides (Merck / Sigma-Aldrich) were commercially available as 1M solutions in toluene or THF and used as received. Gas chromatography was performed on a Bruker Scion 436-GC with a TCD detector. GC-MS analyses were performed on a Bruker Scion 436-GC with a Scion SQ-MS mass spectrometry detector. NMR analyses were performed on a Bruker Fourier 300 MHz or Bruker Avance III HD 400 MHz spectrometer and referenced to the solvent residual peak.
Dideuteriodiphenylgermane Ph_2GeD_2 was synthesised as described in the literature.[39]
Elemental analyses were performed using Thermo Scientific FLASH 2000 analyser. For oxygen content pyrolytic reactor was used. Presented values are averages of two combustions.

1.3. Representative procedure of hydrogermylation

A Schlenk bomb flask, previously oven dried and filled with argon, was charged with 1.0 mmol of germane, 1.0 mmol of alkene, 0.1 mL of mesitylene, and 1.0 mL of dry toluene. A GC reference sample of approx. 30 µL was drawn and 0.1 mL of 1M $NaHB(s\text{-}Bu)_3$ solution was added. A magnetic stirring bar was placed into the reaction mixture, and the vessel was closed with a PTFE plug valve. The vessel was then placed in an oil bath preheated to 100 °C and the heating continued for 24 hours. After this time, the vessel was cooled down and another GC sample was taken. To isolate the product, a portion of 5 ml of n-hexane was first added to the reaction mixture. After 60 minutes of stirring, the suspension was filtered through a 0.45 µm syringe filter and the filtrate was evaporated *in vacuo*. The crude product was purified by a chromatography column using a mixture of hexane and diethyl ether (9:1 v/v) as the eluent and SiO_2 silanized with chloro(dimethyl)octylsilane as stationery phase.

1.4. Catalytic trial with benzylsodium

Benzylsodium solution was obtained as described in the literature.[40]

A solution of dried chlorobenzene (0.203 mL, 0.252 g, 2.25 mmol) in 3 mL of dry toluene was placed in a previously evacuated and filled with argon 25 mL flask with integrated air condenser, an inert gas bubbler, and a side arm. To this solution was added 0.115 g (5.0 mmol) of sodium freshly chopped into flakes under inert atmosphere. The mixture was then stirred under the flow of argon and without heating for approximately 3 h, when initially rising temperature started to drop. It was then placed in an oil bath preheated to 115 °C and refluxed for 2 h. After cooling down to approximately 70 C, 200 µL of the resulting solution was drawn and used to induce activity in a typical reaction system comprising 1.0 mmol of diphenylgermane and 1.0 mmol of styrene. It was found out that after 8 h at 100 °C, the conversion of Ph_2GeH_2 was 40%.

Detailed description of DFT calculations

As the beginning of the theoretical investigation, we attempted to build a general description of chemical entities that could determine mentioned regioselectivity of the reaction. It appeared natural that styrene should be activated by a nucleophilic attack on or an electrophilic attack from the terminal carbon atom in order to form a carbocation or a carbanion stabilized by resonance (as described in our preceding research).[13] Hence, we expected a nucleophilic or electrophilic germanium species to be generated in the initial phase of the reaction. Only one of a number of ideas produced a coherent, stepwise pathway: one that would start with the reaction between $NaHBMe_3$ and $PhGeH_3$ and generate BMe_3, molecular hydrogen and sodium dihydro(phenyl)germanide $NaPhGeH_2$.[41] However, despite $NaPhGeH_2$ being formed more easily than $NaPhSiH_2$, this mechanism still required overcoming a much higher energy barrier than styrene activation ($\Delta\Delta G$ > 30 kcal/mol) and did not provide a satisfactory explanation of reaction regioselectivity. Other concepts, such as generation of $Na[PhGeH_4]$, concerted reaction with 6-membered transition state, and formation of $(PhGeH_3)_2$, did not produce complete reaction pathways and had to be ruled out. These computations were a further confirmation of a previously drawn conclusion that regardless of the final regioselectivity, the reaction was initiated by a nucleophilic attack of a hydride anion from $NaHBMe_3$ on the terminal carbon atom of styrene (Figure 1, **M** suffix), which is preferred over the attack on benzylic carbon (**aM** suffix). The observations for phenylgermane are almost identical as for phenylsilane; Chart 1 is introduced to give a picture of relative energies within the methodology applied in this study.

The explanation arrived with the subsequent step and the two different geometries of collision between the $PhCH^{-}CH_3$ carbanion (**4M**) and phenylgermane (Chart 2). One possibility involves the

attack of the lone electron pair on germanium atom and the formation of a pentacoordinate germanium species with a new C-Ge bond (**5M**-**7M**). In the other one, which has been discarded in our previous studies due to much higher energy barriers in the case of reaction of $PhSiH_3$, the same electron pair attacks a hydrogen atom in $PhGeH_3$, rendering the aforementioned sodium dihydro(phenyl)germanide $NaPhGeH_2$ (**5M**-**8L**). While we are fully aware that the carbanion can also attack BMe_3 molecule released beforehand (this species was described in one of our previous papers),[13] we do not discuss it here in detail for a number of reasons. First, this potential B-C bond still has to be broken in order to create a C-Ge or C-H bond; therefore, the relative energy differences between the two pathways of interest are not affected largely by such simplification; at the same time, computational complexity is significantly reduced. Moreover, our recent findings[42] elicit a supposition that due to a low concentration of free triethylborane in the reaction mixture, at least some portion of product molecules can result from a different mechanism in which $NaHBMe_3$ acts merely as an initiator.

If the pentacoordinate germanium anion **7M** is formed, one of the hydrogen atoms bonded to germanium is removed to render the final product **11M**. This can be done by a BMe_3 molecule, regenerating $NaHBMe_3$ (**8M**-**10M**), which re-enters the cycle and acts as a catalyst, a mechanism that has already been identified in our research. We also wanted to verify whether the hydrogen atom can be removed directly by another styrene molecule (**8S**-**10S**), starting a new cycle at **4M**. This would eliminate the necessity for scarce BMe_3 in favor of styrene, which constitutes a much more abundant component of the reaction mixture, at least in the initial phase of the reaction.

The last pathway that should be discussed, and the most fundamental one for hydrogermylation mechanism discussed herein, proceeds after sodium dihydro(phenyl)germanide **8L** is formed. This species attacks a styrene molecule at the terminal carbon atom and produces a carbanion (**9L**-**11L**). The latter is again a secondary, resonance-stabilized one; this time, however, the germanium atom is at an anti-Markovnikov position. The final product **15L** is released after this carbanion abstracts a hydrogen cation from phenylgermane (**12L**-**14L**) and produces sodium dihydro(phenyl)germanide for a subsequent cycle.

The analysis of Figure 2 delivers a precise explanation for the anti-Markovnikov mode of reaction between phenylgermane and styrene. Starting from **5M**, a barrier of only ca. 10.7 kcal/mol (**6L**) has to be overcome to generate $NaPhGeH_2$ (**7L**); this can be viewed as the point of no return as the reverse reaction would require ca. 31 kcal/mol. When it comes to the Markovnikov mode, three barriers can be distinguished: 3.1 kcal/mol (pentavalent germanium anion **7M**), 13.1 kcal/mol (weak complex with BMe_3 **8M**) and 7.8 kcal/mol (abstraction of hydrogen by BMe_3 **9M**); the subsequent drop in Gibbs free energy by 37.0 kcal/mol would also prevent reverse reaction. For a direct hydrogen transfer from pentavalent germanium to styrene, these three steps require 3.1 kcal/mol (**7M**), 6.1 kcal/mol (weak complex with styrene **8S**) and 21.9 kcal/mol (hydrogen transfer **9S**). These energy barriers explain well why $NaPhGeH_2$ is generated and enters the anti-Markovnikov catalytic cycle. The cycle itself includes two transition states of 16.7 kcal/mol (styrene activation **10L**; relative to preceding stationary point) and 12.7 kcal/mol (sodium dihydro(phenyl)germanide regeneration **13L**); the former is much lower than activation of styrene by $NaHBMe_3$ (23.3 kcal/mol) and provides a convincing explanation for the anti-Markovnikov mode of reaction. Gibbs free energy profiles display similar features for diphenylgermane (Chart 3, transition states of 15.7 kcal/mol and 13.6 kcal/mol in the anti-Markovnikov cycle) and triethylgermane (Chart 4, 17.4 kcal/mol and 18.2 kcal/mol); it is worth noting that energies are generally 5-10 kcal/mol higher for the latter than for (di)phenylgermane (relative to isolated substrates).

Finding a new reaction pathway leading to anti-Markovnikov product created the necessity to revisit our previous research on hydrosilylation in order to verify if they are not contradictory. Chart 5

presents Gibbs free energy profiles for anti-Markovnikov and Markovnikov pathways (including the cycle with styrene abstracting hydrogen from pentavalent silicon). In this model, the Markovnikov mode presents three energy barriers from **5M** to **10M** that are almost identical to those for hydrogermylation: 1.7 kcal/mol (**7M**), 13.2 kcal/mol (**8M**) and 7.8 kcal/mol (**9M**), followed by energy decrease by 34.9 kcal/mol (the styrene pathway **8S-10S** is again disfavoured). The anti-Markovnikov mode, on the other hand, presents a significantly higher energy barrier than for germanium, i.e. 14.8 kcal/mol (**6L**), and a smaller decrease by 25.8 kcal/mol (**7L**). The anti-Markovnikov cycle would also involve much higher energy barriers of 21.0 kcal/mol (**10L**) and 17.1 kcal/mol (**13L**). Chart 6 gives an accurate picture of Gibbs free energy differences for anti-Markovnikov hydrogermylation (observed experimentally) and anti-Markovnikov hydrosilylation (not observed experimentally). It should be stressed that although Gibbs free energy profiles match perfectly the experimental outcome of both hydrosilylation and hydrogermylation, we are aware of other factors that can impact the course of reaction. Two of them are especially worth noting: the low concentration of free BMe_3, which favours the anti-Markovnikov mode (where BMe_3 is unnecessary), and the geometry of collision between carbanion $PhCH^{-}CH_3$ and phenylgermane/phenylsilane, which favours the Markovnikov mode (C-Si and C-Ge bonds in **7M** are formed much more easily than **6L** transition state).

3. Analytical data of isolated products

3.1. Phenethyldiphenylgermane, 1

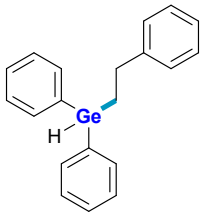

Off-white waxy solid, 240 mg (72%)
^{1}H NMR (400 MHz, Chloroform-d) δ 7.56 – 7.02 (m, 20H), 5.26 (t, J = 3.2 Hz, 1H), 2.85 – 2.76 (m, 2H), 1.66 – 1.56 (m, 2H).
^{13}C NMR (101 MHz, Chloroform-d) δ 144.04, 136.51, 134.84, 129.96 – 124.98 (m), 31.91, 15.35.

MS (EI, 70 eV), m/z (% rel. abund.): 334 (0.8, M^+ *isotopologue*), 333 (0.7, M^+ *isotopologue*), 229 (100), 227 (69), 230 (58), 149 (92), 150 (81), 256 (26), 254 (23), 77 (14), 74 (16)
Elem Anal. (%):Calcd for $C_{20}H_{20}Ge$: C: 72.14, H: 6.05 (C/H = 11.92); Found: C: 69.30, H: 5.83, N < LOD, O: 0.07 (C/H = 11.87); Corresponds to 96% purity

3.2. (2-(Naphthalen-2-yl)ethyl)diphenylgermane, 2

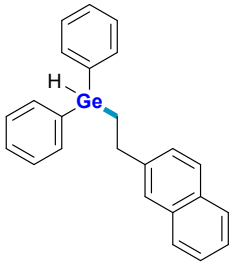

Off-white solid, 310 mg (82%)
^{1}H NMR (400 MHz, Benzene-d6) δ 7.69 – 7.04 (m, 20H), 5.22 (t, J = 3.2 Hz, 1H), 2.91 – 2.83 (m, 2H), 1.61 (ddd, J = 11.7, 5.6, 3.2 Hz, 2H).
^{13}C NMR (101 MHz, Benzene-d6) δ 141.44, 137.20 – 131.96 (m), Ge 129.50 – 124.54 (m), 32.00, 15.13.
MS (EI, 70 eV), m/z (% rel. abund.): 384 (7, M^+ *isotopologue*), 385 (5, M^+ *isotopologue*), 383 (4, M^+ *isotopologue*), 227 (100), 229 (96), 226 (79), 152 (68), 150 (64), 149 (58), 77 (16)
Elem Anal. (%): Calcd for $C_{24}H_{22}Ge$: C: 75.25, H: 5.79 (C/H = 13.00); Found: C: 73.76, H: 5.67, N < LOD, O: <LOD (C/H = 13.01); Corresponds to 98% purity

3.3. (4-Methoxyphenethyl)diphenylgermane, 3

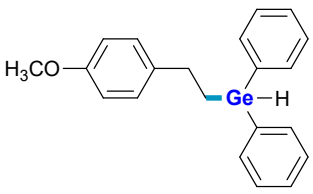

Off-white solid, 273 mg, 75%
^{1}H NMR (400 MHz, Benzene-d6) δ 7.60 – 6.69 (m, 14H), 5.20 (t, J = 3.2 Hz, 1H), 3.33 (s, 3H), 2.77 – 2.71 (m, 2H), 1.56 (ddd, J = 11.6, 5.8, 3.3 Hz, 2H).

^{13}C NMR (101 MHz, Benzene-d6) δ 158.20, 136.55, 135.91, 135.12, 134.78, 128.87, 128.82, 128.26, 113.82, 54.44, 31.01, 15.61.

MS (EI, 70 eV), m/z (% rel. abund.): 364(3, M^+ *isotopologue*), 365 (3, M^+ *isotopologue*), 135 (100), 150 (63), 151 (63), 229 (56), 227 (56), 149 (53), 136 (29), 79 (27), 77 (26)
Elem Anal. (%): Calcd for $C_{21}H_{22}GeO$: C: 69.48, H: 6.11, O: 4.41 (C/H = 11.37, C/O = 15.76); Found: C: 68.09, H: 5.96, N < LOD, O: 4.37 (C/H = 11.46, C/O = 15.58); Corresponds to 98% purity

*3.4. (2,2-diphenylethyl)diphenylgermane, **4***

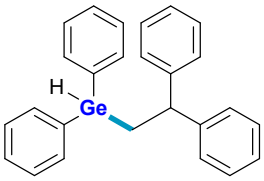

Pale yellow solid, 217 mg, 53%
^{1}H NMR (300 MHz, Benzene-d6) δ 7.61 – 6.85 (m, 20H), 5.00 (t, J = 3.4 Hz, 1H), 4.15 (t, J = 8.2 Hz, 1H), 2.03 (dd, J = 8.2, 3.4 Hz, 2H).
^{13}C NMR (101 MHz, Benzene-d6) δ 146.10, 135.70, 129.56 – 124.89, 48.22, 21.52.
MS (EI, 70 eV), m/z (% rel. abund.): 409 (0.6, M^+ *isotopologue*), 408 (0.3, M^+ *isotopologue*), 410 (0.3, M^+ *isotopologue*), 229 (100), 230 (64), 227 (60), 149 (45), 151 (37), 150 (49), 332 (26), 333 (23), 331 (21), 77 (21);
Elem Anal. (%): Calcd for $C_{26}H_{24}Ge$: C: 76.33, H: 5.91 (C/H = 12.92); Found: C: 74.04, H: 5.76, N < LOD, O: < LOD (C/H = 12.85); Corresponds to 97% purity

*3.5. Diphenyl(2-phenylpropyl)germane, **5***

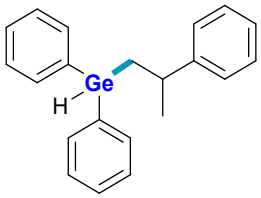

White waxy solid, 153 mg, 44%
^{1}H NMR (300 MHz, Benzene-d6) δ 7.21 – 6.61 (m, 27H), 4.86 (t, J = 3.5 Hz, 1H), 2.67 (h, J = 7.1 Hz, 1H), 1.46 – 1.22 (m, 2H), 0.97 (d, J = 6.9 Hz, 3H).
^{13}C NMR (101 MHz, Benzene-d6) δ 148.51, 137.00, 136.85, 134.76, 134.66, 126.64, 125.99, 37.32, 24.91, 23.75.
MS (EI, 70 eV), m/z (% rel. abund.): 347 (0.3, M^+ *isotopologue*), 346 (0.3, M^+ *isotopologue*), 345 (0.3, M^+ *isotopologue*), 348 (0.2, M^+ *isotopologue*), 227 (100), 229 (95), 226 (77), 149 (53), 150 (45), 152 (44), 270 (23), 271 (22), 79 (21), 77 (18)
Elem Anal. (%): Calcd for $C_{21}H_{22}Ge$: C: 72.68, H: 6.39 (C/H = 11.37); Found: C: 71.94, H: 6.35, N < LOD, O: < LOD (C/H = 11.33); Corresponds to 99% purity

3.6. (2-(naphthalen-2-yl)ethyl)(phenyl)germane, 6

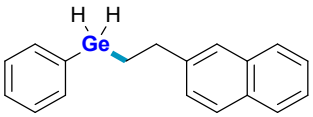

Off-white waxy solid, 110 mg (36%)

^{1}H NMR (300 MHz, Chloroform-d) δ 7.99 – 7.01 (m, 12H), 4.35 (t, J = 3.2 Hz, 1H), 2.94 – 2.87 (m, 1H), 1.52 (ddt, J = 11.4, 6.2, 3.2 Hz, 2H).

MS (EI, 70 eV), m/z (% rel. abund.): 307 (13, M^+ *isotopologue*), 308 (12, M^+ *isotopologue*), 306 (7, M^+ *isotopologue*), 156 (100), 155 (74), 152 (53), 157 (42), 129 (42), 127 (29), 150 (25), 229 (22), 230 (21), 228 (19), 75 (18), 130 (16);

Elem Anal. (%): Calcd for $C_{18}H_{18}Ge$: C: 70.46, H: 5.91 (C/H = 11.92); Found: C: 66.92, H: 5.62, N < LOD, O: 0.21 (C/H = 11.91); Corresponds to 95% purity

4. Charts

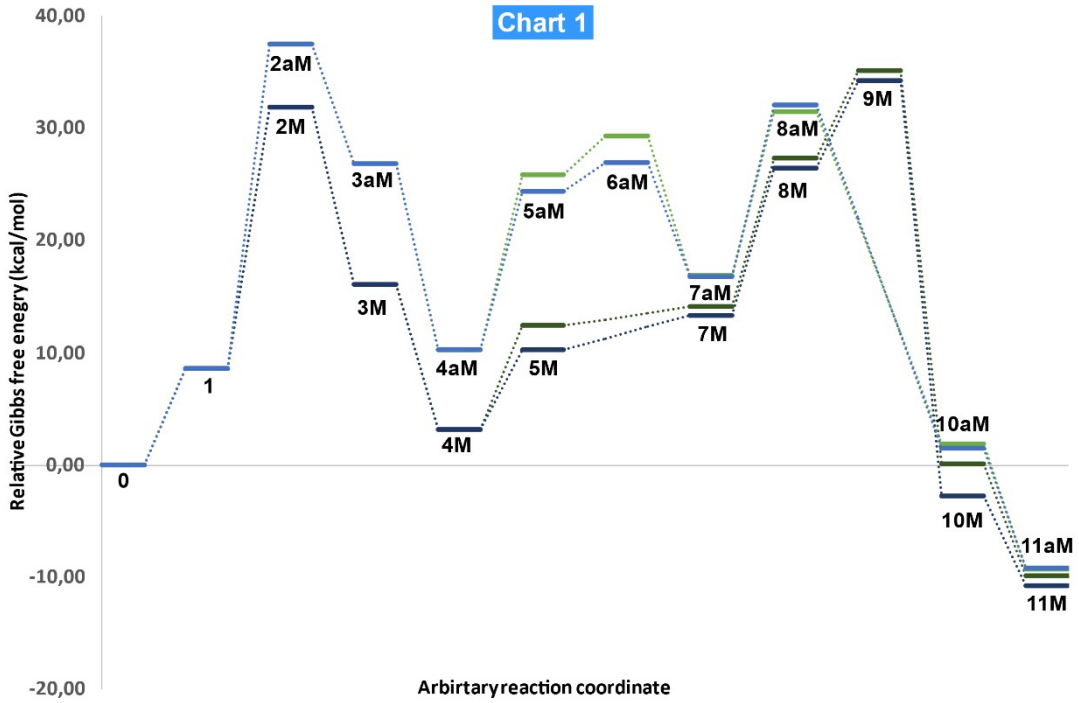

0	2M	3M	4M	5M		7M	8M	9M	10M	11M
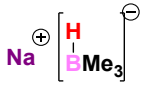	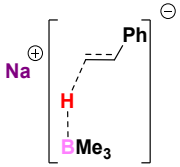	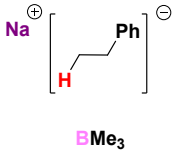	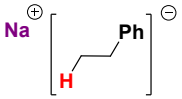	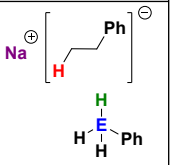		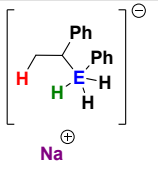	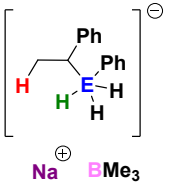	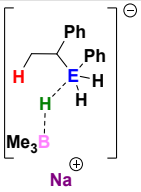	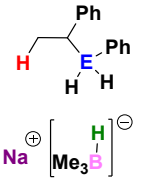	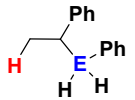
0.00	31.85	16.08	3.11	10.27 (E=Ge) 12.40 (E=Si)		13.32 (E=Ge) 14.09 (E=Si)	26.46 (E=Ge) 27.29 (E=Si)	34.24 (E=Ge) 35.08 (E=Si)	-2.80 (E=Ge) 0.15 (E=Si)	-10.71 (E=Ge) -9.91 (E=Si)

1	2aM	3aM	4aM	5aM	6aM	7aM	8aM		10aM	11aM
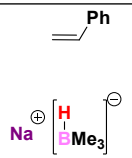	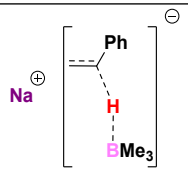	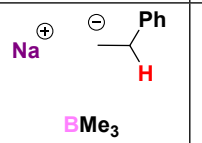	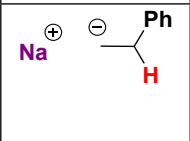	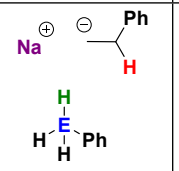	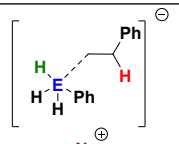	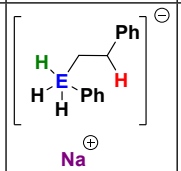	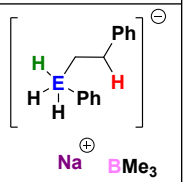		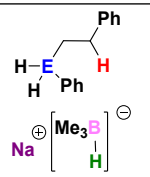	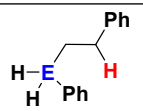

8.59	37.53	26.87	10.26	24.39 (E=Ge) 25.84 (E=Si)	26.92 (E=Ge) 29.26 (E=Si)	16.76 (E=Ge) 16.83 (E=Si)	32.08 (E=Ge) 31.43 (E=Si)

1.46 (E=Ge) 1.85 (E=Si)	-9.22 (E=Ge) -9.28 (E=Si)

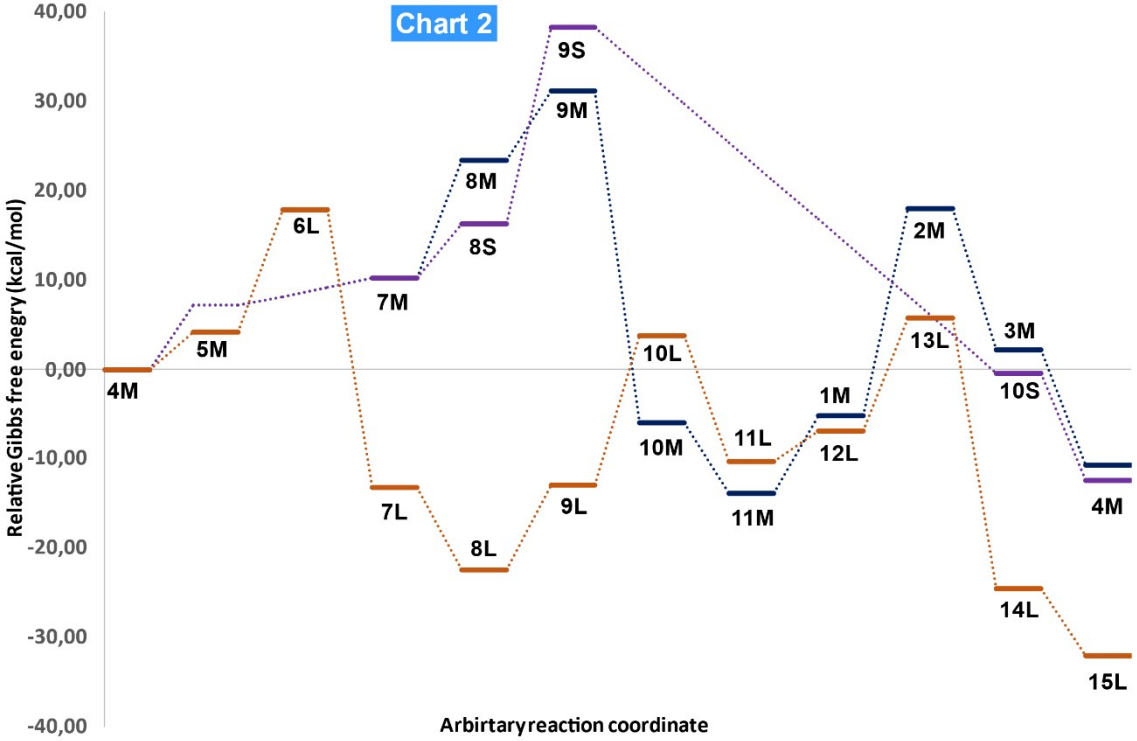

4M	For structures see above	0.00
5M		7.16
7M		10.21
8M		23.35
9M		31.13
10M		-5.91
11M		-13.83
1		-5.23
2M		18.02
3M		2.25
4M (next cycle)		-10.71

6L	7L	8L	9L	10L	11L	12L	13L	14L	15L
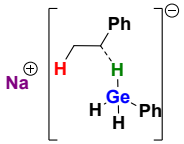	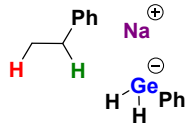	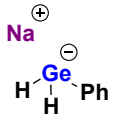	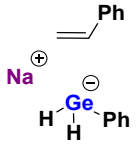	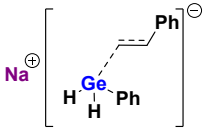	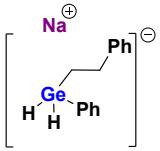	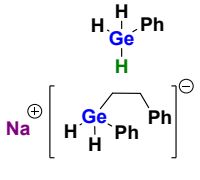	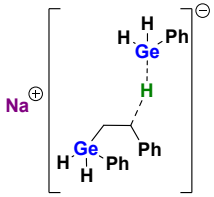	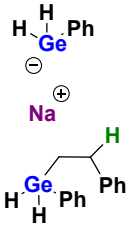	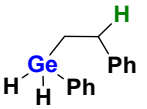
17.81	-13.25	-22.46	-12.87	3.83	-10.33	-6.94	5.80	-24.45	-31.95

8S	9S	10S
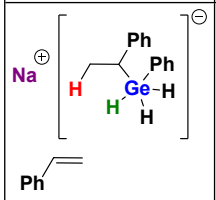	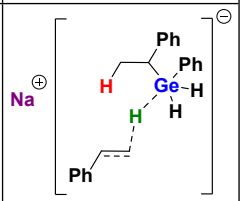	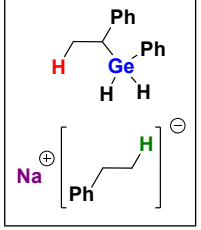

16.30	38.22

-0.39

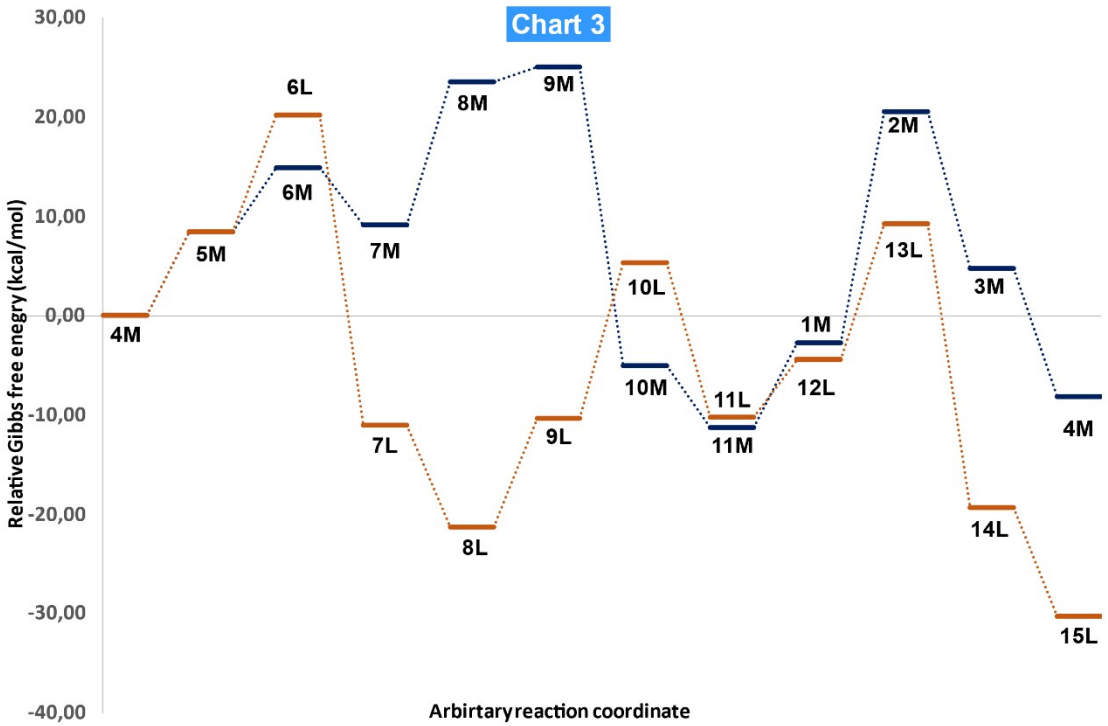

4M	6L	7L	8L	9L	10L	11L	12L	13L	14L	15L
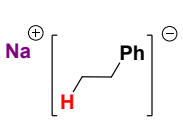	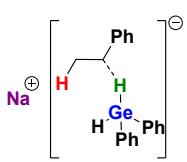	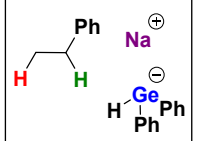	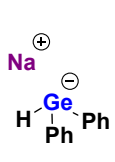	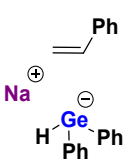	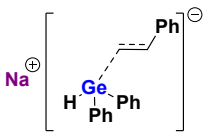	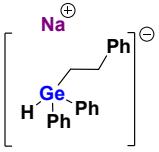	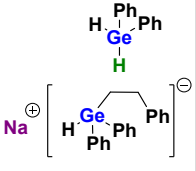	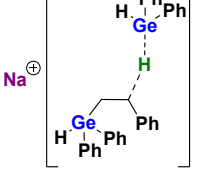	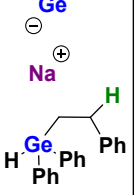	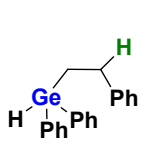
0.00	20.15	-11.04	-21.31	-10.35	5.35	-10.22	-4.44	9.20	-19.27	-30.20

5M	6M	7M	8M	9M	10M	11M	1M	2M	3M	4M
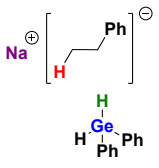	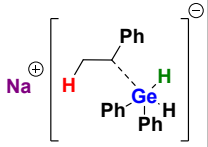	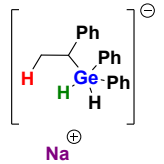	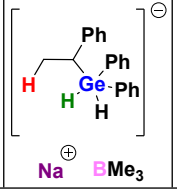	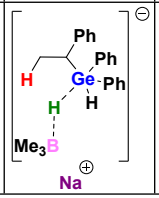	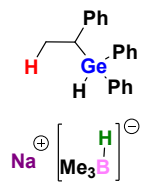	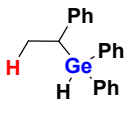	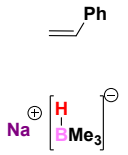	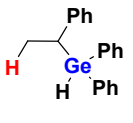	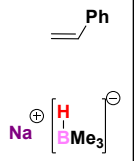	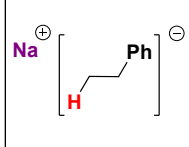

8.47	14.87	9.09	23.52	25.02	-5.09	-11.30	-2.71	20.55	4.78	-8.18

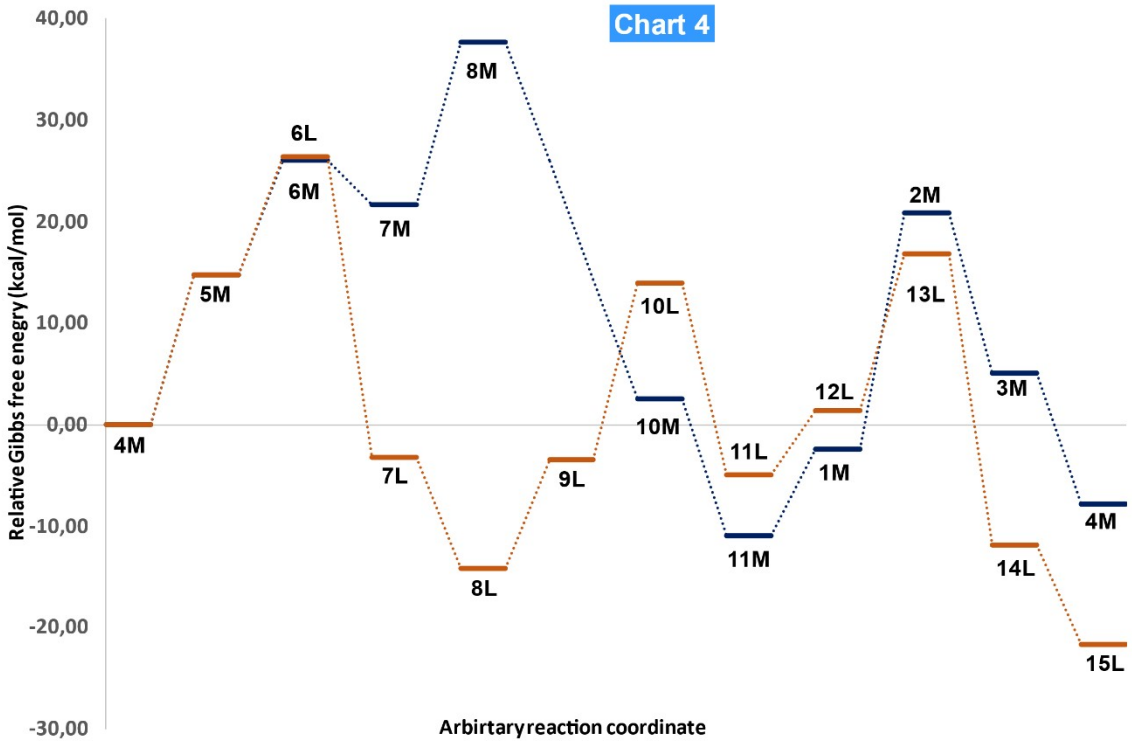

4M	6L	7L	8L	9L	10L	11L	12L	13L	14L	15L
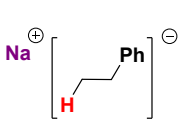	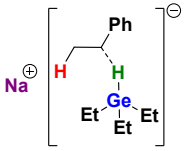	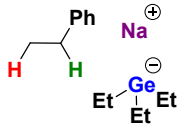	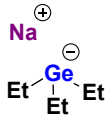	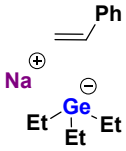	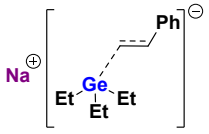	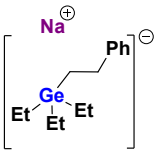	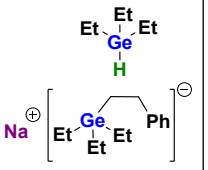	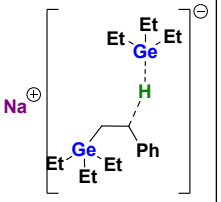	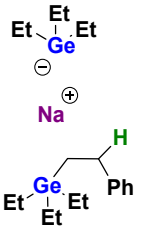	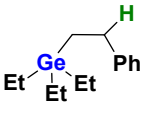
0.00	26.36	-3.22	-14.13	-3.43	13.94	-4.90	1.37	16.79	-11.79	-21.61
5M	6M	7M	8M		10M	11M	1M	2M	3M	4M

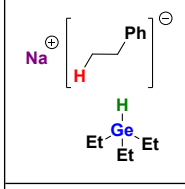	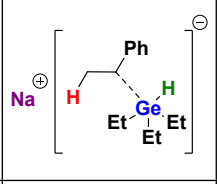	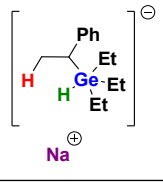	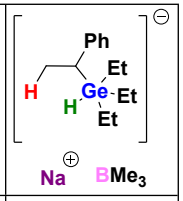
14.77	25.99	21.63	37.65

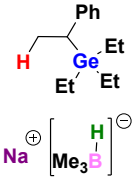	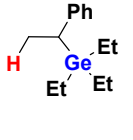	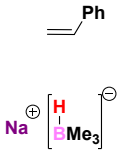	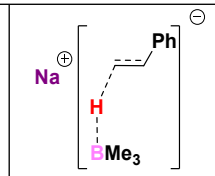	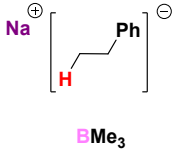	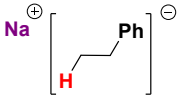
2.52	-10.95	-2.36	20.89	5.12	-7.84

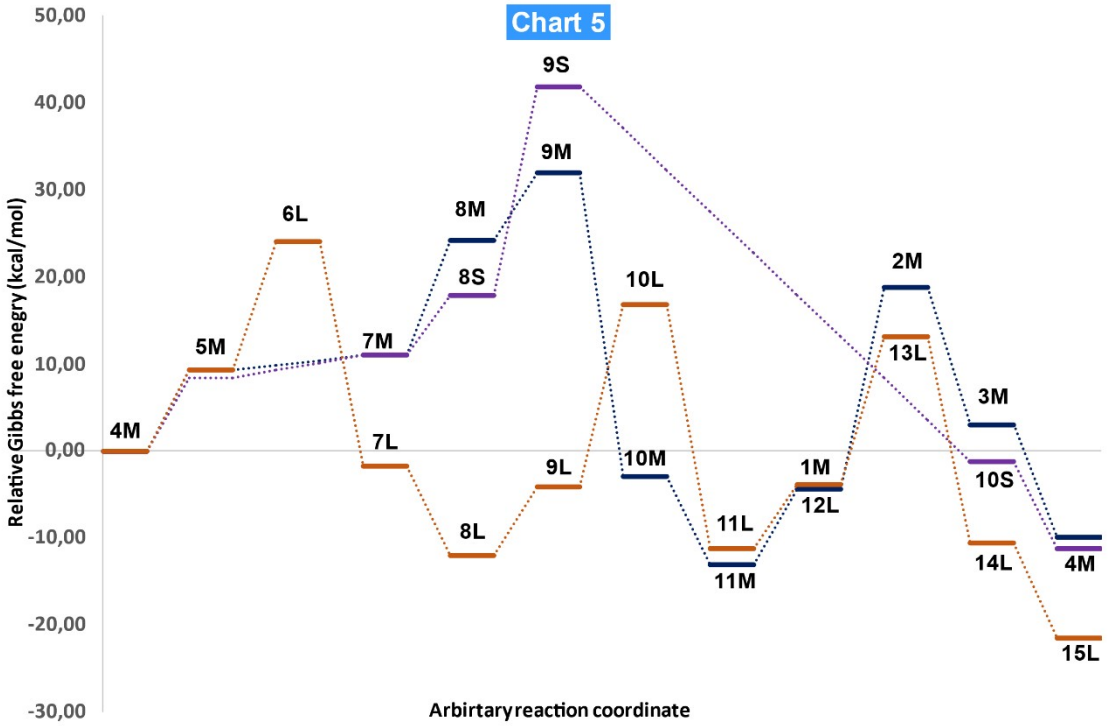

8S	9S	10S
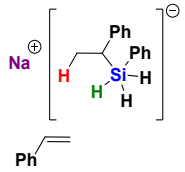	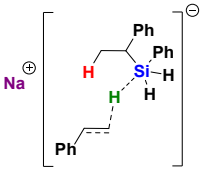	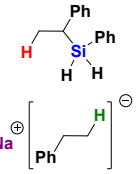
17.89	41.81	-1.25

4M	6L	7L	8L	9L	10L	11L	12L	13L	14L	15L
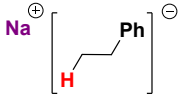	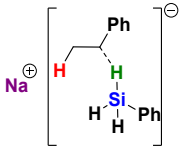	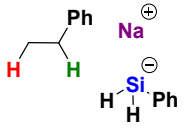	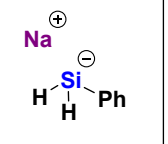	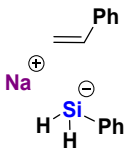	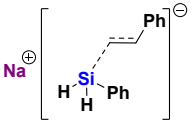	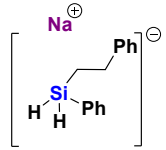	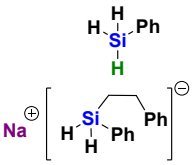	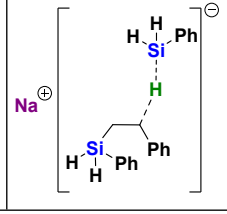	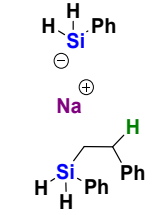	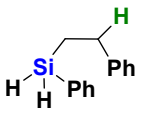

0.00	24.10	-1.74	-12.00	-4.16	16.81	-11.20	-3.91	13.14	-10.50	-21.54
5M		7M	8M	9M	10M	11M	1M	2M	3M	4M
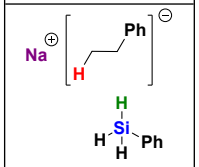		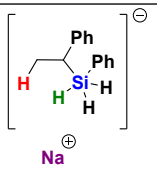	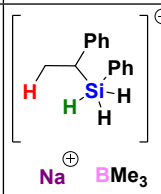	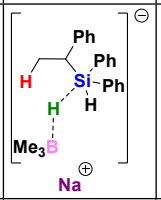	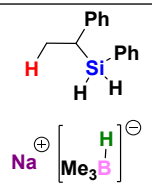	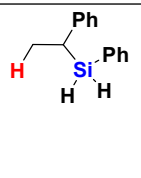	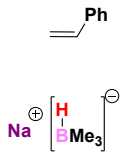	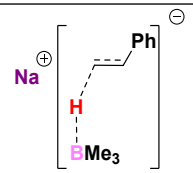	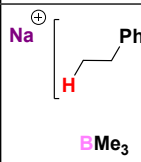	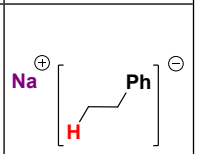
9.29		10.98	24.18	31.96	-2.97	-13.02	-4.43	18.82	3.05	-9.91

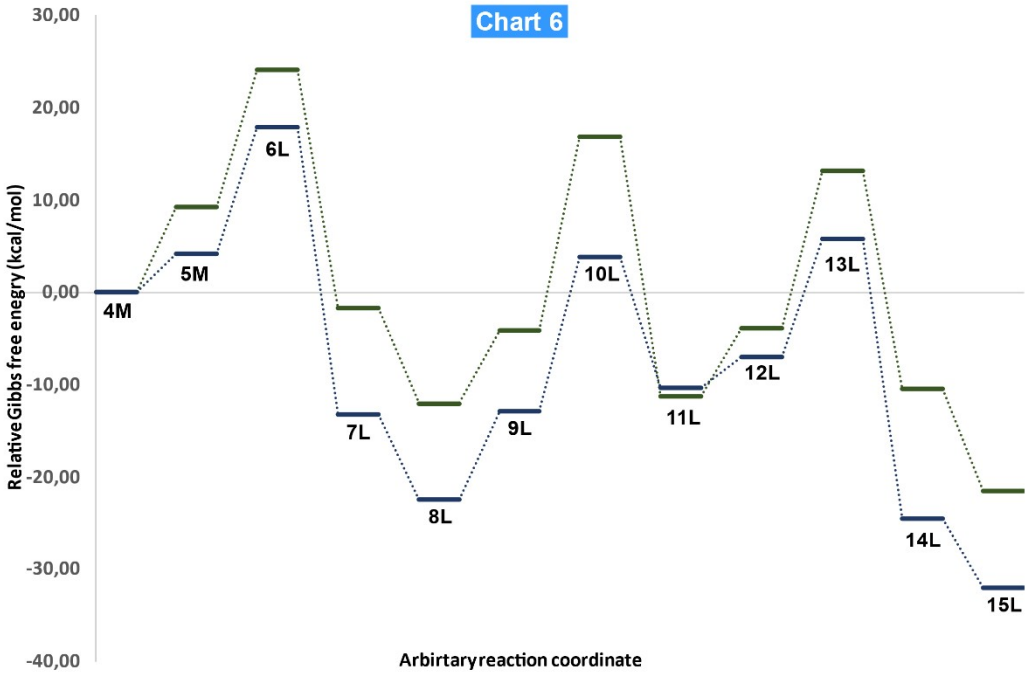

	4M	5M	6L	7L	8L	9L	10L	11L
	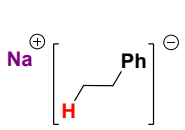	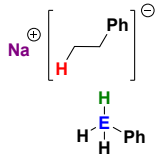	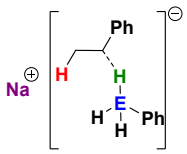	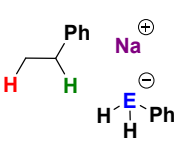	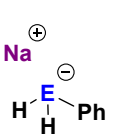	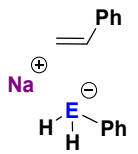	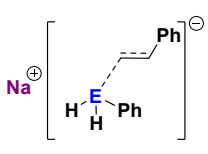	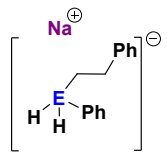
E=Si	0.00	9.29	24.10	-1.74	-12.00	-4.16	16.81	-11.20
E=Ge		4.20	17.81	-13.25	-22.46	-12.87	3.83	-10.33

	12L	13L	14L	15L
	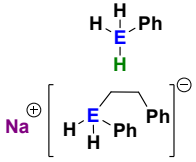	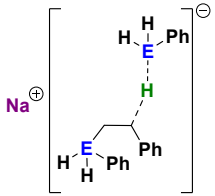	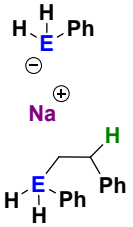	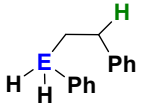
E=Si	-3.91	13.14	-10.50	-21.54
E=Ge	-6.94	5.80	-24.45	-31.95

5. NMR Spectra

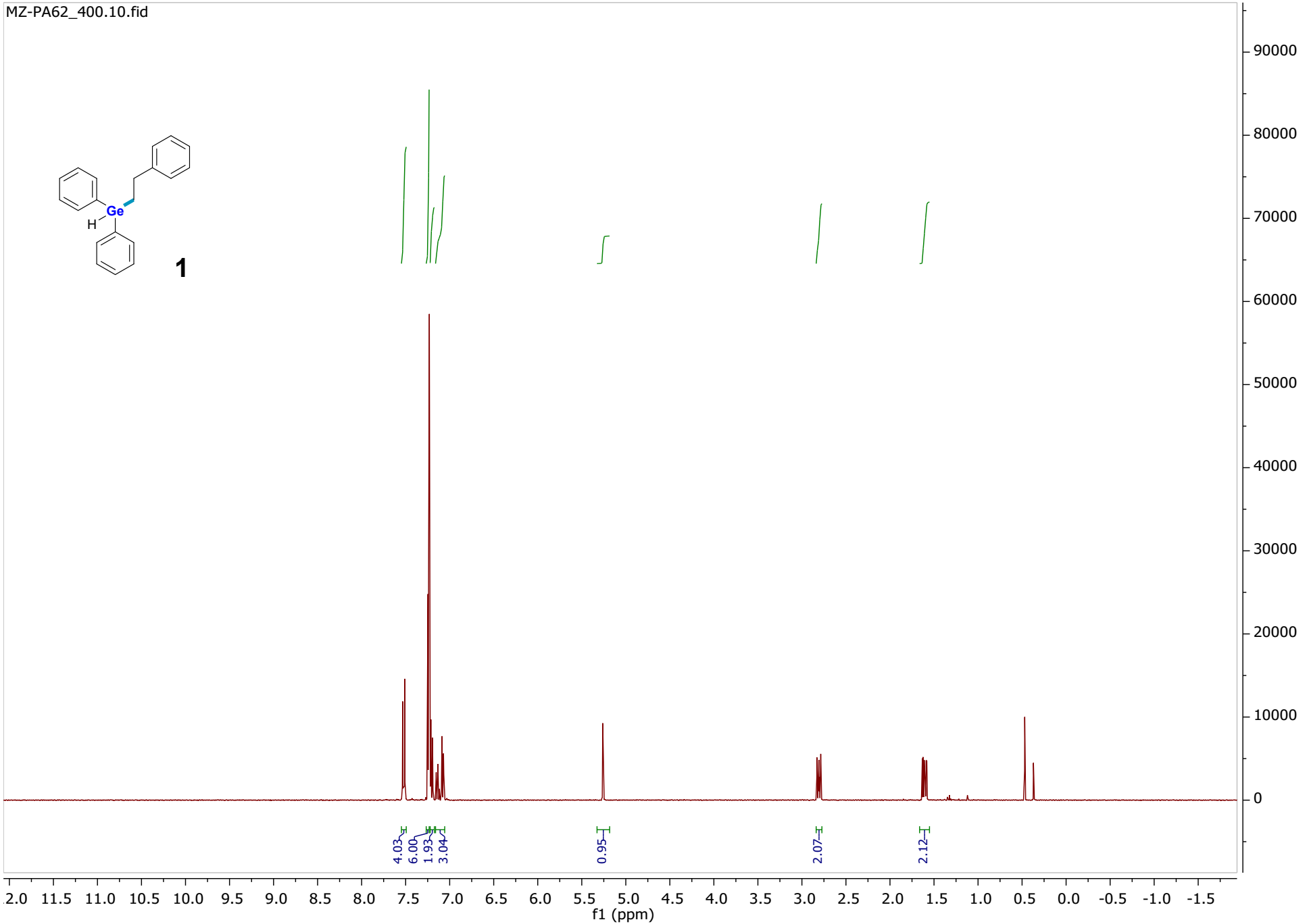

MZ-PA62_400.11.fid

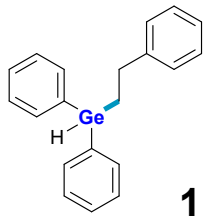

1

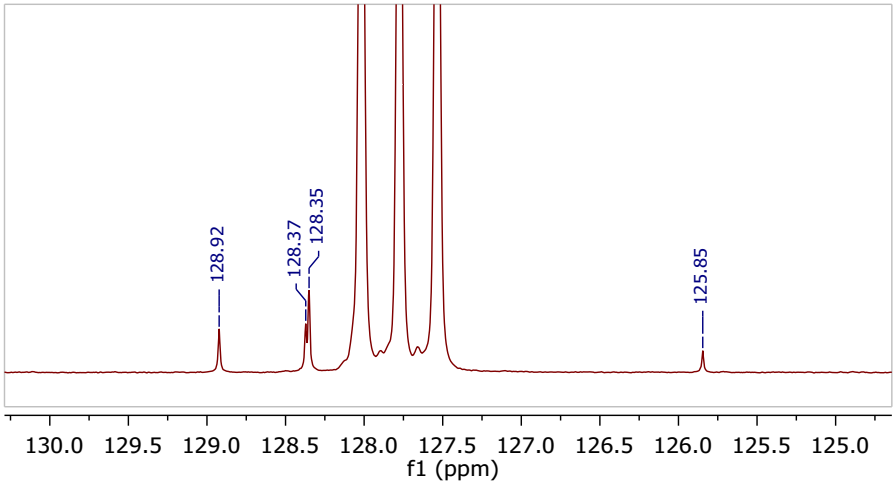

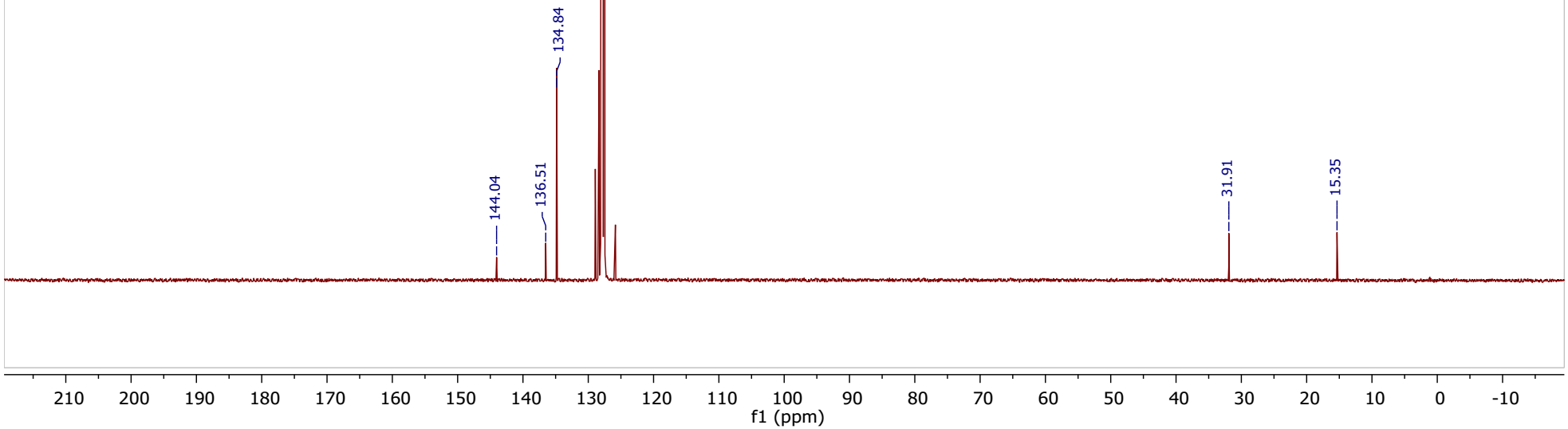

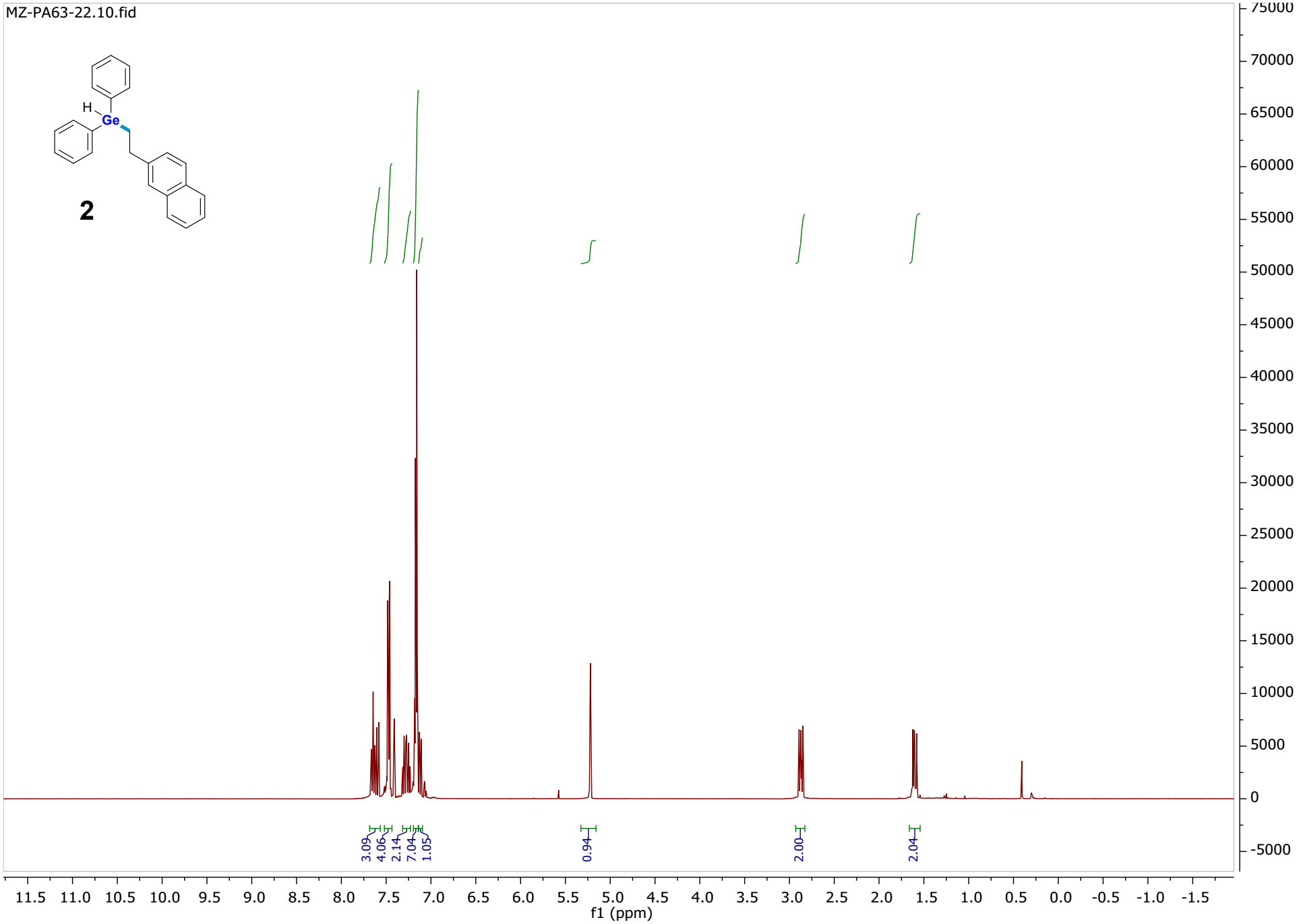
MZ-PA63-22.10.fid
H
Ge
2
3.09
4.06
2.14
7.04
1.05
0.94
2.00
2.04
f1 (ppm)

MZ-PA63-22.11.fid

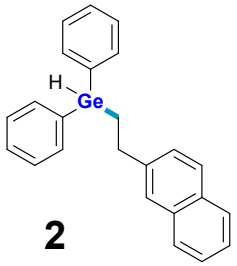

2

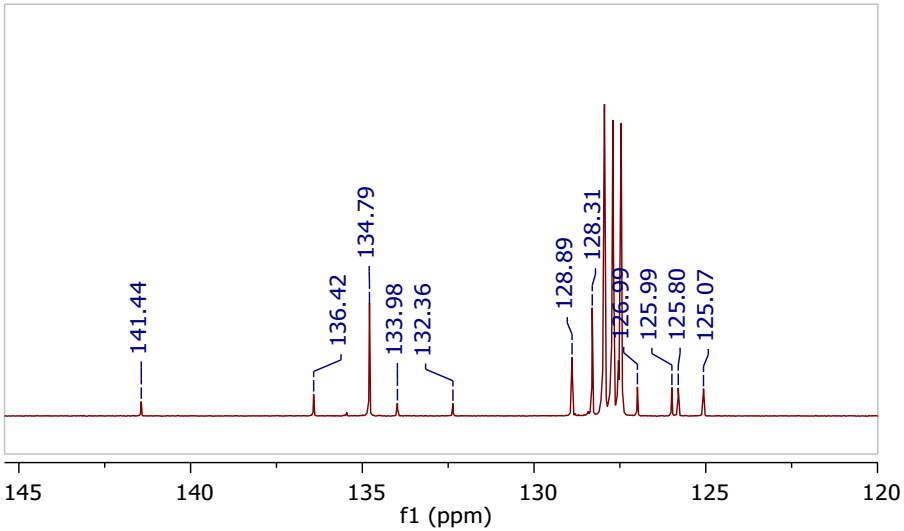

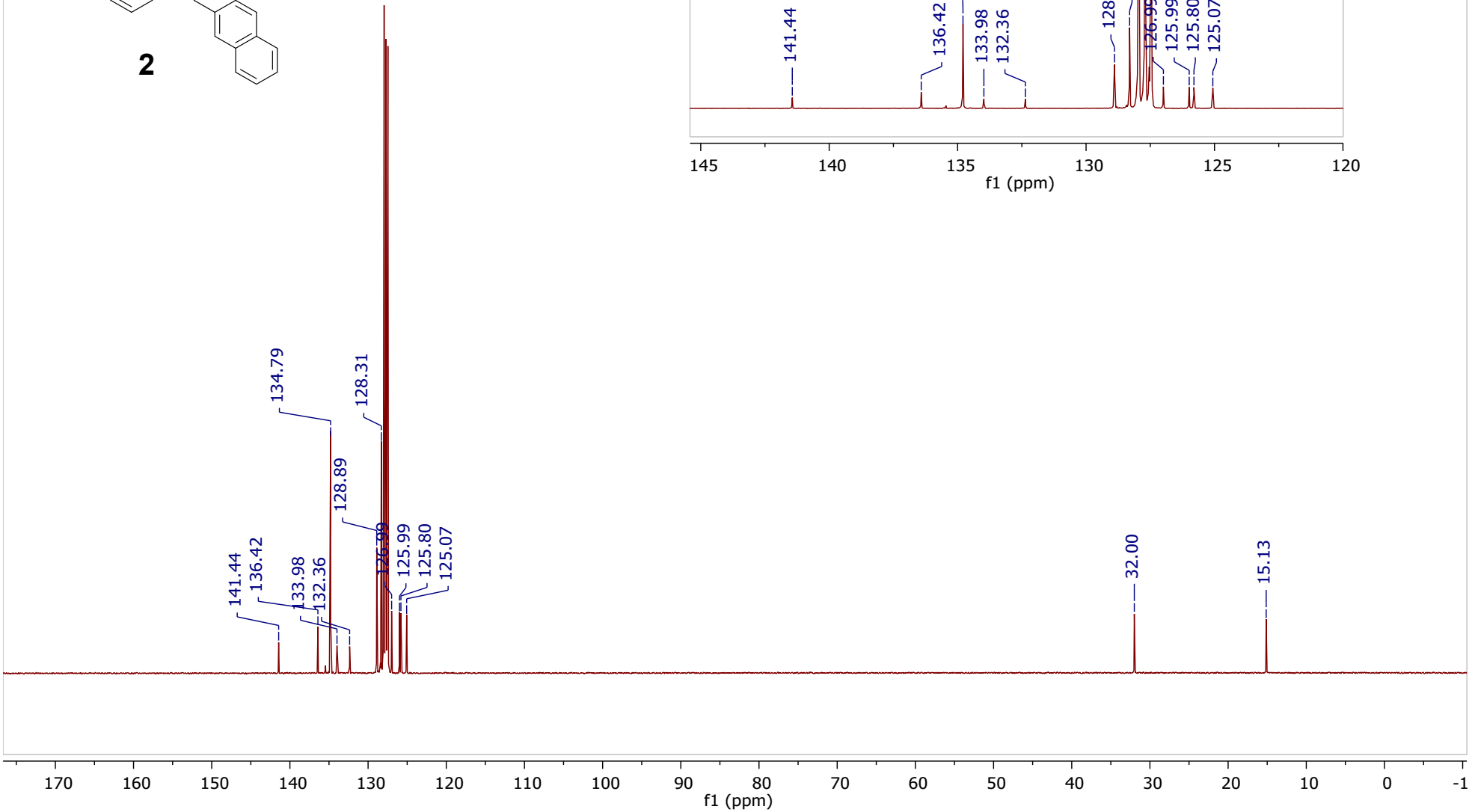

MZ-PA-65-6-7_400.10.fid

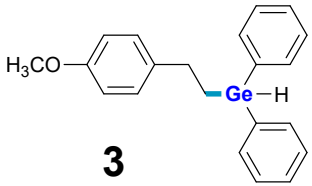

3

MZ-PA-65-6-7_400.11.fid

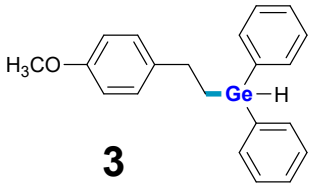

3

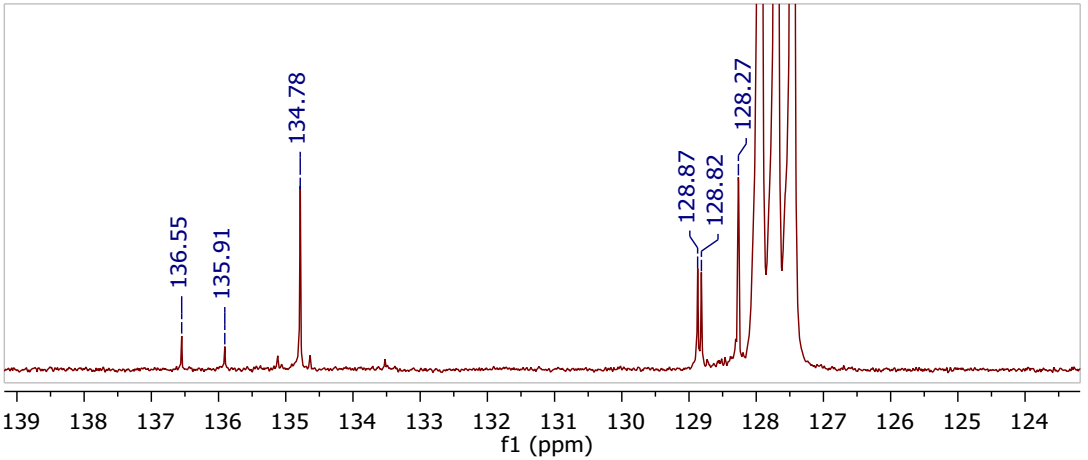

MZ-PA61-23.10.fid
PROTON32 C6D6 {C:\IconNMR\mzar} mzar 14

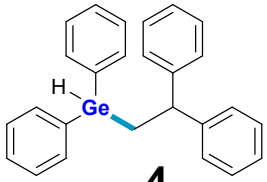

4

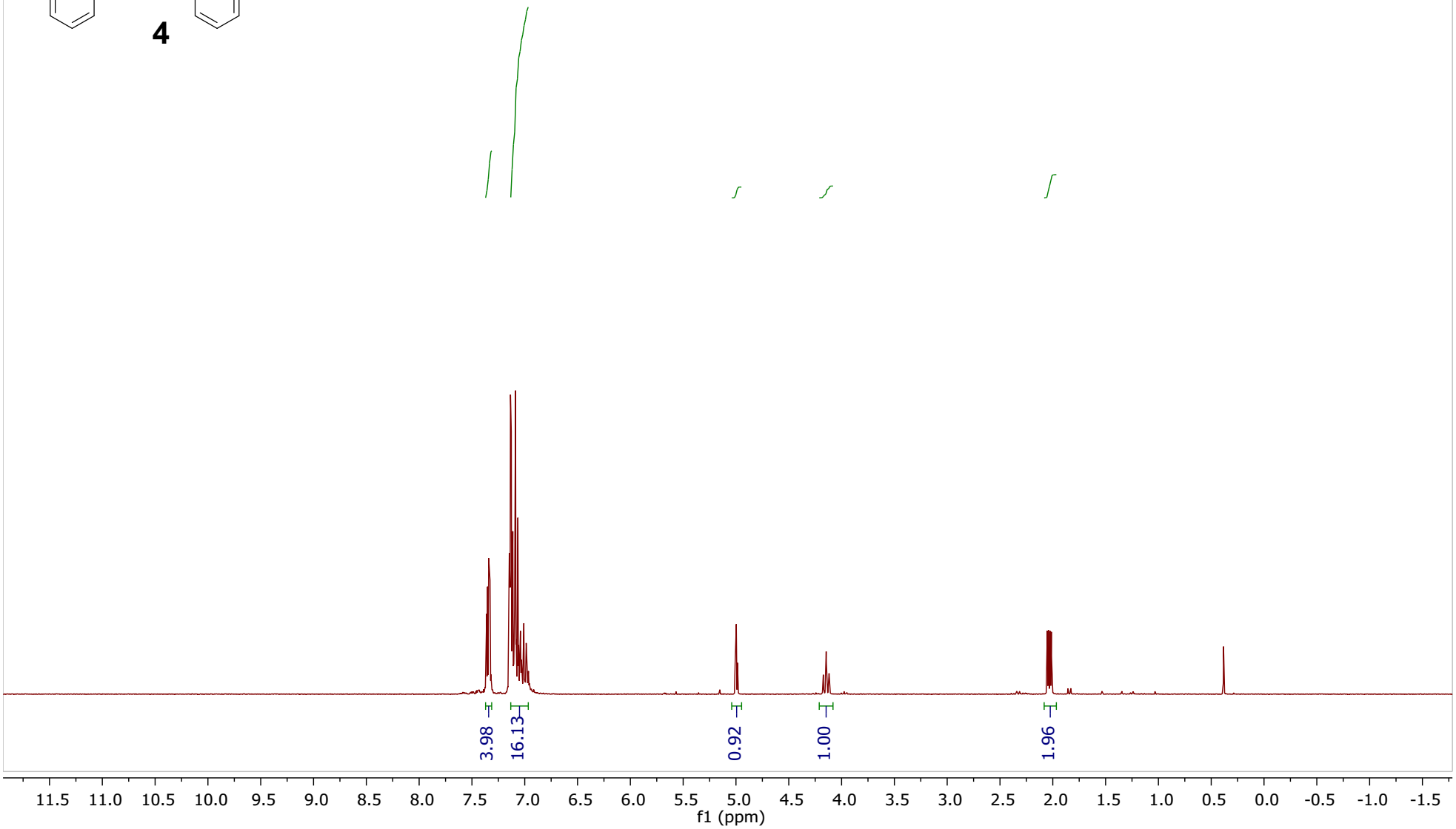

MZ-PA61.10.fid

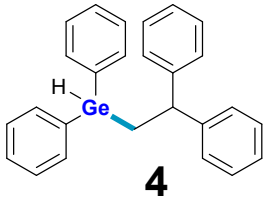

4

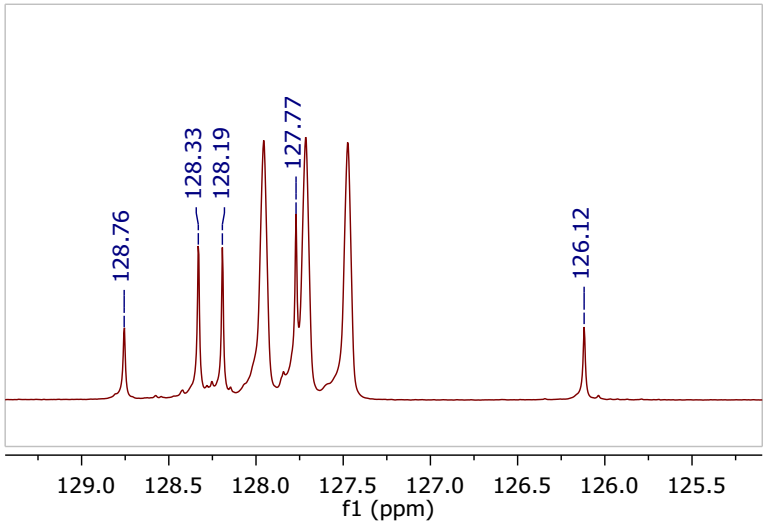

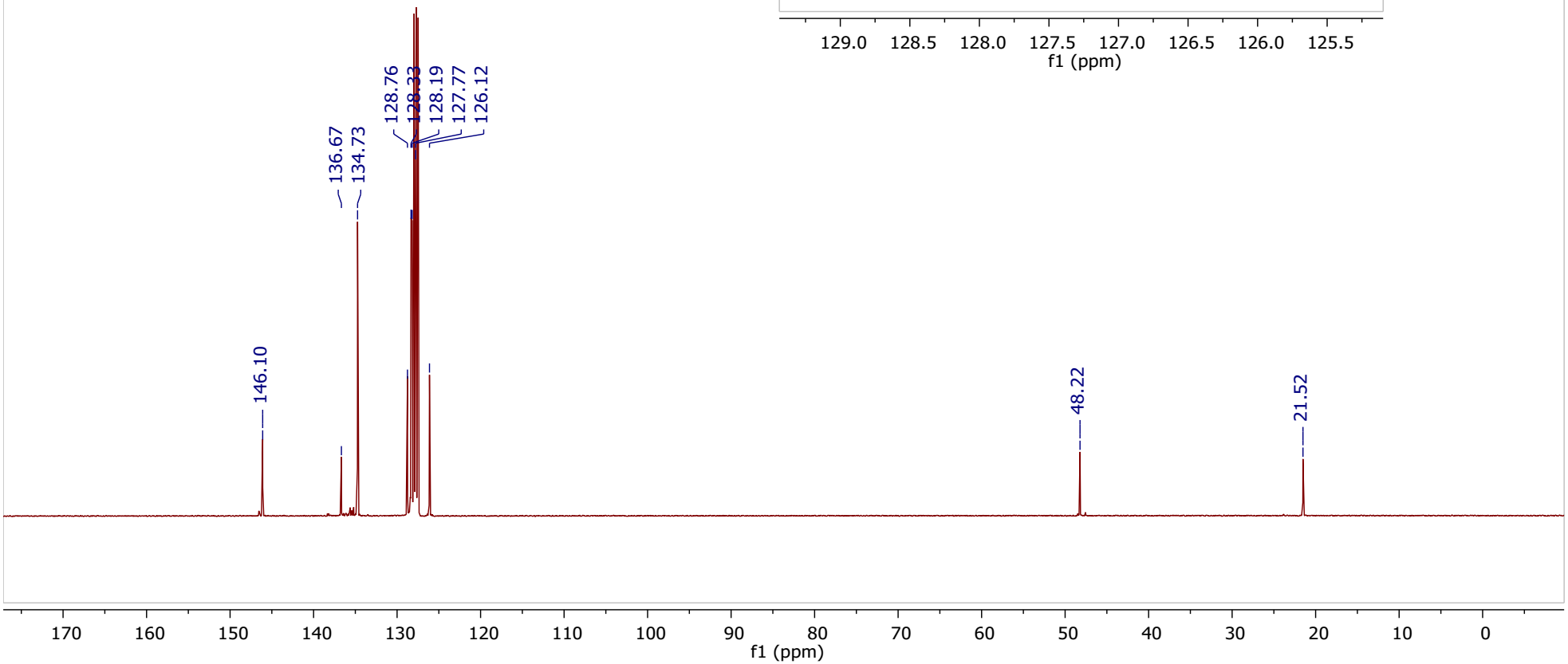

MZ-PA66-14.20.fid
PROTON_64 C6D6 {C:\IconNMR\PP_group} PP_group 11

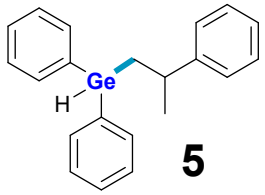

5

MZ-PA19.10.fid
PROTON_64 CDCl3 {C:\IconNMR\mzar} mzar 16

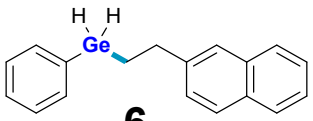

6

References

(1) Rappe, A. K.; Casewit, C. J.; Colwell, K. S.; Goddard, W. A.; Skiff, W. M. UFF, a Full Periodic Table Force Field for Molecular Mechanics and Molecular Dynamics Simulations. *J. Am. Chem. Soc.* **1992**, *114* (25), 10024–10035. https://doi.org/10.1021/ja00051a040.

(2) Zhao, Y.; Truhlar, D. G. The M06 Suite of Density Functionals for Main Group Thermochemistry, Thermochemical Kinetics, Noncovalent Interactions, Excited States, and Transition Elements: Two New Functionals and Systematic Testing of Four M06-Class Functionals and 12 Other Functionals. *Theor. Chem. Acc.* **2008**, *120* (1–3), 215–241. https://doi.org/10.1007/s00214-007-0310-x.

(3) Clark, T.; Chandrasekhar, J.; Spitznagel, G. W.; Schleyer, P. V. R. Efficient Diffuse Function-Augmented Basis Sets for Anion Calculations. III. The 3-21+G Basis Set for First-Row Elements, Li-F. *J. Comput. Chem.* **1983**, *4* (3), 294–301. https://doi.org/10.1002/jcc.540040303.

(4) Dill, J. D.; Pople, J. A. Self-consistent Molecular Orbital Methods. XV. Extended Gaussian-type Basis Sets for Lithium, Beryllium, and Boron. *J. Chem. Phys.* **1975**, *62* (7), 2921–2923. https://doi.org/10.1063/1.430801.

(5) Ditchfield, R.; Hehre, W. J.; Pople, J. A. Self-Consistent Molecular-Orbital Methods. IX. An Extended Gaussian-Type Basis for Molecular-Orbital Studies of Organic Molecules. *J. Chem. Phys.* **1971**, *54* (2), 724–728. https://doi.org/10.1063/1.1674902.

(6) Francl, M. M.; Pietro, W. J.; Hehre, W. J.; Binkley, J. S.; Gordon, M. S.; DeFrees, D. J.; Pople, J. A. Self-consistent Molecular Orbital Methods. XXIII. A Polarization-type Basis Set for Second-row Elements. *J. Chem. Phys.* **1982**, *77* (7), 3654–3665. https://doi.org/10.1063/1.444267.

(7) Gordon, M. S.; Binkley, J. S.; Pople, J. A.; Pietro, W. J.; Hehre, W. J. Self-Consistent Molecular-Orbital Methods. 22. Small Split-Valence Basis Sets for Second-Row Elements. *J. Am. Chem. Soc.* **1982**, *104* (10), 2797–2803. https://doi.org/10.1021/ja00374a017.

(8) Hariharan, P. C.; Pople, J. A. The Influence of Polarization Functions on Molecular Orbital Hydrogenation Energies. *Theor. Chim. Acta* **1973**, *28* (3), 213–222. https://doi.org/10.1007/BF00533485.

(9) Hehre, W. J.; Ditchfield, R.; Pople, J. A. Self—Consistent Molecular Orbital Methods. XII. Further Extensions of Gaussian—Type Basis Sets for Use in Molecular Orbital Studies of Organic Molecules. *J. Chem. Phys.* **1972**, *56* (5), 2257–2261. https://doi.org/10.1063/1.1677527.

(10) Spitznagel, G. W.; Clark, T.; von Ragué Schleyer, P.; Hehre, W. J. An Evaluation of the Performance of Diffuse Function-Augmented Basis Sets for Second Row Elements, Na-Cl. *J. Comput. Chem.* **1987**, *8* (8), 1109–1116. https://doi.org/10.1002/jcc.540080807.

(11) Check, C. E.; Faust, T. O.; Bailey, J. M.; Wright, B. J.; Gilbert, T. M.; Sunderlin, L. S. Addition of Polarization and Diffuse Functions to the LANL2DZ Basis Set for P-Block Elements. *J. Phys. Chem. A* **2001**, *105* (34), 8111–8116. https://doi.org/10.1021/jp011945l.

(12) Wadt, W. R.; Hay, P. J. Ab Initio Effective Core Potentials for Molecular Calculations. Potentials for Main Group Elements Na to Bi. *J. Chem. Phys.* **1985**, *82* (1), 284–298. https://doi.org/10.1063/1.448800.

(13) Nowicki, M.; Zaranek, M.; Pawluć, P.; Hoffmann, M. DFT Study of Trialkylborohydride-Catalysed Hydrosilylation of Alkenes-the Mechanism and Its Implications. *Catal. Sci. Technol.* **2020**, *10* (4), 1066–1072. https://doi.org/10.1039/c9cy02261a.

(14) Peng, C.; Bernhard Schlegel, H. Combining Synchronous Transit and Quasi-Newton Methods to Find Transition States. *Isr. J. Chem.* **1993**, *33* (4), 449–454. https://doi.org/10.1002/ijch.199300051.

(15) Fukui, K. The Path of Chemical Reactions - the IRC Approach. *Acc. Chem. Res.* **1981**, *14* (12), 363–368. https://doi.org/10.1021/ar00072a001.

(16) Barone, V.; Cossi, M.; Tomasi, J. A New Definition of Cavities for the Computation of Solvation Free Energies by the Polarizable Continuum Model. *J. Chem. Phys.* **1997**, *107* (8), 3210–3221. https://doi.org/10.1063/1.474671.

(17) Cossi, M.; Barone, V.; Cammi, R.; Tomasi, J. Ab Initio Study of Solvated Molecules: A New Implementation of the Polarizable Continuum Model. *Chem. Phys. Lett.* **1996**, *255* (4–6), 327–335. https://doi.org/10.1016/0009-2614(96)00349-1.

(18) Pascual-ahuir, J. L.; Silla, E.; Tuñon, I. GEPOL: An Improved Description of Molecular Surfaces.

III. A New Algorithm for the Computation of a Solvent-Excluding Surface. *J. Comput. Chem.* **1994**, *15* (10), 1127–1138. https://doi.org/10.1002/JCC.540151009.
(19) Miertuš, S.; Tomasi, J. Approximate Evaluations of the Electrostatic Free Energy and Internal Energy Changes in Solution Processes. *Chem. Phys.* **1982**, *65* (2), 239–245. https://doi.org/10.1016/0301-0104(82)85072-6.
(20) Miertuš, S.; Scrocco, E.; Tomasi, J. Electrostatic Interaction of a Solute with a Continuum. A Direct Utilizaion of AB Initio Molecular Potentials for the Prevision of Solvent Effects. *Chem. Phys.* **1981**, *55* (1), 117–129. https://doi.org/10.1016/0301-0104(81)85090-2.
(21) Cancès, E.; Mennucci, B.; Tomasi, J. A New Integral Equation Formalism for the Polarizable Continuum Model: Theoretical Background and Applications to Isotropic and Anisotropic Dielectrics. *J. Chem. Phys.* **1997**, *107* (8), 3032–3041. https://doi.org/10.1063/1.474659.
(22) Mennucci, B.; Tomasi, J. Continuum Solvation Models: A New Approach to the Problem of Solute's Charge Distribution and Cavity Boundaries. *J. Chem. Phys.* **1997**, *106* (12), 5151–5158. https://doi.org/10.1063/1.473558.
(23) Mennucci, B.; Cancès, E.; Tomasi, J. Evaluation of Solvent Effects in Isotropic and Anisotropic Dielectrics and in Ionic Solutions with a Unified Integral Equation Method: Theoretical Bases, Computational Implementation, and Numerical Applications. *J. Phys. Chem. B* **1997**, *101* (49), 10506–10517. https://doi.org/10.1021/jp971959k.
(24) Barone, V.; Cossi, M. Quantum Calculation of Molecular Energies and Energy Gradients in Solution by a Conductor Solvent Model. *J. Phys. Chem. A* **1998**, *102* (11), 1995–2001. https://doi.org/10.1021/jp9716997.
(25) Cossi, M.; Barone, V.; Mennucci, B.; Tomasi, J. Ab Initio Study of Ionic Solutions by a Polarizable Continuum Dielectric Model. *Chem. Phys. Lett.* **1998**, *286* (3–4), 253–260. https://doi.org/10.1016/S0009-2614(98)00106-7.
(26) Barone, V.; Cossi, M.; Tomasi, J. Geometry Optimization of Molecular Structures in Solution by the Polarizable Continuum Model. *J. Comput. Chem.* **1998**, *19* (4), 404–417. https://doi.org/10.1002/(SICI)1096-987X(199803)19:4<404::AID-JCC3>3.0.CO;2-W.
(27) Cossi, M.; Barone, V. Solvent Effect on Vertical Electronic Transitions by the Polarizable Continuum Model. *J. Chem. Phys.* **2000**, *112* (5), 2427–2435. https://doi.org/10.1063/1.480808.
(28) Cossi, M.; Rega, N.; Scalmani, G.; Barone, V. Polarizable Dielectric Model of Solvation with Inclusion of Charge Penetration Effects. *J. Chem. Phys.* **2001**, *114* (13), 5691–5701. https://doi.org/10.1063/1.1354187.
(29) Cossi, M.; Scalmani, G.; Rega, N.; Barone, V. New Developments in the Polarizable Continuum Model for Quantum Mechanical and Classical Calculations on Molecules in Solution. *J. Chem. Phys.* **2002**, *117* (1), 43–54. https://doi.org/10.1063/1.1480445.
(30) Cossi, M.; Rega, N.; Scalmani, G.; Barone, V. Energies, Structures, and Electronic Properties of Molecules in Solution with the C-PCM Solvation Model. *J. Comput. Chem.* **2003**, *24* (6), 669–681. https://doi.org/10.1002/jcc.10189.
(31) Scalmani, G.; Frisch, M. J. Continuous Surface Charge Polarizable Continuum Models of Solvation. I. General Formalism. *J. Chem. Phys.* **2010**, *132* (11), 114110. https://doi.org/10.1063/1.3359469.
(32) Lipparini, F.; Scalmani, G.; Mennucci, B.; Cancès, E.; Caricato, M.; Frisch, M. J. A Variational Formulation of the Polarizable Continuum Model. *J. Chem. Phys.* **2010**, *133* (1), 014106. https://doi.org/10.1063/1.3454683.
(33) Caricato, M. Absorption and Emission Spectra of Solvated Molecules with the EOM–CCSD–PCM Method. *J. Chem. Theory Comput.* **2012**, *8* (11), 4494–4502. https://doi.org/10.1021/ct3006997.
(34) Tomasi, J.; Mennucci, B.; Cammi, R. Quantum Mechanical Continuum Solvation Models. *Chem. Rev.* **2005**, *105* (8), 2999–3094. https://doi.org/10.1021/cr9904009.
(35) Boys, S. F.; Bernardi, F. The Calculation of Small Molecular Interactions by the Differences of Separate Total Energies. Some Procedures with Reduced Errors. *Mol. Phys.* **1970**, *19* (4), 553–566. https://doi.org/10.1080/00268977000101561.
(36) Simon, S.; Duran, M.; Dannenberg, J. J. How Does Basis Set Superposition Error Change the Potential Surfaces for Hydrogen-bonded Dimers? *J. Chem. Phys.* **1996**, *105* (24), 11024–11031. https://doi.org/10.1063/1.472902.
(37) Gaussian 16, Revision C.01, M. J. Frisch, G. W. Trucks, H. B. Schlegel, G. E. Scuseria, M. A.

Robb, J. R. Cheeseman, G. Scalmani, V. Barone, G. A. Petersson, H. Nakatsuji, X. Li, M. Caricato, A. V. Marenich, J. Bloino, B. G. Janesko, R. Gomperts, B. Mennucci, H. P. Hratchian, J. V. Ortiz, A. F. Izmaylov, J. L. Sonnenberg, D. Williams-Young, F. Ding, F. Lipparini, F. Egidi, J. Goings, B. Peng, A. Petrone, T. Henderson, D. Ranasinghe, V. G. Zakrzewski, J. Gao, N. Rega, G. Zheng, W. Liang, M. Hada, M. Ehara, K. Toyota, R. Fukuda, J. Hasegawa, M. Ishida, T. Nakajima, Y. Honda, O. Kitao, H. Nakai, T. Vreven, K. Throssell, J. A. Montgomery, Jr., J. E. Peralta, F. Ogliaro, M. J. Bearpark, J. J. Heyd, E. N. Brothers, K. N. Kudin, V. N. Staroverov, T. A. Keith, R. Kobayashi, J. Normand, K. Raghavachari, A. P. Rendell, J. C. Burant, S. S. Iyengar, J. Tomasi, M. Cossi, J. M. Millam, M. Klene, C. Adamo, R. Cammi, J. W. Ochterski, R. L. Martin, K. Morokuma, O. Farkas, J. B. Foresman, and D. J. Fox, Gaussian, Inc., Wallingford CT, 2016.

(38) Pritchard, B. P.; Altarawy, D.; Didier, B.; Gibson, T. D.; Windus, T. L. New Basis Set Exchange: An Open, Up-to-Date Resource for the Molecular Sciences Community. *J. Chem. Inf. Model.* **2019**, *59* (11), 4814–4820. https://doi.org/10.1021/acs.jcim.9b00725.

(39) Durig, J. R.; Turner, J. B.; Gibson, B. M.; Sink, C. W. The Vibrational Spectra and Structure of Organogermanes. VII. Low-Wavenumber Vibrations of Some Diphenyl-Germanes. *J. Mol. Struct.* **1969**, *4* (1), 79–89. https://doi.org/10.1016/0022-2860(69)85030-1.

(40) Gilman, H.; Pacevitz, H. A.; Baine, O. Benzylalkali Compounds. *J. Am. Chem. Soc.* **1940**, *62* (6), 1514–1520. https://doi.org/10.1021/ja01863a054.

(41) Birchall, T.; Drummond, I. Nuclear Magnetic Resonance Spectra of Phenylsilane, Phenylgermane, and Their Anions: Comments on the Relative Acidities of Phenylgermane and Germane. *J. Chem. Soc. A Inorganic, Phys. Theor.* **1970**, 1401. https://doi.org/10.1039/j19700001401.

(42) Nowicki, M.; Kuciński, K.; Hreczycho, G.; Hoffmann, M. Catalytic and Non-Catalytic Hydroboration of Carbonyls: Quantum-Chemical Studies. *Org. Biomol. Chem.* **2021**, *19* (13), 3004–3015. https://doi.org/10.1039/D1OB00037C.